University of Nebraska - Lincoln

DigitalCommons@University of Nebraska - Lincoln

Robert Powers Publications

Published Research - Department of Chemistry

1992

^{1}H, ^{15}N, ^{13}C, and ^{13}CO Assignments of Human Interleukin-4 Using Three-Dimensional Double- and Triple-Resonance Heteronuclear Magnetic Resonance Spectroscopy

Robert Powers
University of Nebraska - Lincoln, rpowers3@unl.edu

Daniel S. Garrett
Laboratory of Chemical Physics, Building 2, National Institute of Diabetes and Digestive and Kidney Diseases, National Institutes of Health, Bethesda, Maryland

Carl J. March
Laboratory of Chemical Physics, Building 2, National Institute of Diabetes and Digestive and Kidney Diseases, National Institutes of Health, Bethesda, Maryland

Eric A. Frieden
Laboratory of Chemical Physics, Building 2, National Institute of Diabetes and Digestive and Kidney Diseases, National Institutes of Health, Bethesda, Maryland

Angela M. Gronenborn
Laboratory of Chemical Physics, Building 2, National Institute of Diabetes and Digestive and Kidney Diseases, National Institutes of Health, Bethesda, Maryland

See next page for additional authors

Authors

Robert Powers, Daniel S. Garrett, Carl J. March, Eric A. Frieden, Angela M. Gronenborn, and G. Marius Clore

¹H, ¹⁵N, ¹³C, and ¹³CO Assignments of Human Interleukin-4 Using Three-Dimensional Double- and Triple-Resonance Heteronuclear Magnetic Resonance Spectroscopy[†]

Robert Powers,[‡] Daniel S. Garrett,[‡] Carl J. March,[§] Eric A. Frieden,[§] Angela M. Gronenborn,*,[‡] and
G. Marius Clore*,[‡]

Laboratory of Chemical Physics, Building 2, National Institute of Diabetes and Digestive and Kidney Diseases, National Institutes of Health, Bethesda, Maryland 20892, and Immunex Corporation, 51 University Street, Seattle, Washington 98101

ABSTRACT: The assignment of the ¹H, ¹⁵N, ¹³CO, and ¹³C resonances of recombinant human interleukin-4 (IL-4), a protein of 133 residues and molecular mass of 15.4 kDa, is presented based on a series of 11 three-dimensional (3D) double- and triple-resonance heteronuclear NMR experiments. These studies employ uniformly labeled ¹⁵N- and ¹⁵N/¹³C-labeled IL-4 with an isotope incorporation of >95% for the protein expressed in yeast. Five independent sequential connectivity pathways via one-, two-, and three-bond heteronuclear J couplings are exploited to obtain unambiguous sequential assignments. Specifically, CO(i)–N(i+1),NH(i+1) correlations are observed in the HNCO experiment, the C$^\alpha$H(i),C$^\alpha$(i)–N(i+1) correlations in the HCA(CO)N experiment, the C$^\alpha$(i)–N(i+1),NH(i+1) correlations in the HNCA and HN(CO)CA experiments, the C$^\alpha$H(i)–N(i+1),NH(i+1) correlations in the H(CA)NH and HN(CO)HB experiments, and the C$^\beta$H(i)–N(i+1),NH(i+1) correlations in the HN(CO)HB experiments. The backbone intraresidue C$^\alpha$H(i)–¹⁵N(i)–NH(i) correlations are provided by the ¹⁵N-edited Hartmann–Hahn (HOHAHA) and H(CA)NH experiments, the C$^\beta$H(i)–¹⁵N(i)–NH(i) correlations by the ¹⁵N-edited HOHAHA and HNHB experiments, the ¹³C$^\alpha$(i)–¹⁵N(i)–NH(i) correlations by the HNCA experiment, and the C$^\alpha$H(i)–¹³C$^\alpha$(i)–¹³CO(i) correlations by the HCACO experiment. Aliphatic side-chain spin systems are assigned by 3D ¹H–¹³C–¹³C–¹H correlated (HCCH-COSY) and total correlated (HCCH-TOCSY) spectroscopy. Because of the high resolution afforded by these experiments, as well as the availability of multiple sequential connectivity pathways, ambiguities associated with the limited chemical shift dispersion associated with helical proteins are readily resolved. Further, in the majority of cases (88%), four or more sequential correlations are observed between successive residues. Consequently, the interpretation of these experiments readily lends itself to semiautomated analysis which significantly simplifies and speeds up the assignment process. The assignments presented in this paper provide the essential basis for studies aimed at determining the high-resolution three-dimensional structure of IL-4 in solution.

The human cytokine interleukin-4 (IL-4)[1] is a 15.4-kDa protein of 133 residues which plays a key role in the immune and inflammatory systems [see Paul and Ohara (1987) and Yokota et al. (1988) for reviews]. IL-4 regulates B cell proliferation and differentiation and modulates the survival, proliferation, and differentiation of T cells, as well as a wide range of other hematopoietic cell lines. In addition, IL-4 is a potent inducer of cytotoxic T cells which contributes in part to its antitumor activity (Tepper et al., 1989; Golumbek et al., 1991). Other effects of IL-4 include the induction of class I and II MHC molecules, the regulation of expression of the low-affinity F$_c$ receptor of IgE and the enhancement of IgE and IgG1 cell-surface expression and secretion.

In order to obtain an understanding of the mechanism of action of IL-4 and its mode of interaction with its cell-surface receptor, we have initiated structural studies by NMR aimed at determining its three-dimensional structure in solution. The first step in this process, and the focus of the present paper, involves obtaining complete or near complete resonance as-

signments. This provides the essential data needed to extract a large number of short-range interproton distance contacts from NOE measurements, which constitute the main source of geometric information for NMR structure determinations (Wüthrich, 1986, 1989; Clore & Gronenborn, 1987, 1989, 1991a,c). Although IL-4 is by no means the largest protein whose spectrum has been completely assigned, the assignment constituted a particularly challenging task as the chemical shift

dispersion of the IL-4 spectrum is very narrow. Thus, for example, the amide proton resonances are confined to a spectral region of only 2.7 ppm extending from 6.6 to 9.3 ppm; likewise, the lowest field $C^{\alpha}H$ proton resonates at 5.2 ppm, only slightly downfield of the water resonance, and the highest field methyl resonance is located at 0 ppm. This can be attributed to the fact that IL-4 is a mainly helical protein which has no β-sheet structure as deduced from circular dichroism measurements (Curtis et al., 1991; Windsor et al., 1991). Consequently, it would have been extremely difficult to rely on 3D ^{15}N-separated NOESY and HOHAHA experiments (Marion et al., 1989b; Clore & Gronenborn, 1991a) which have been so successfully applied to the sequential assignment of β-sheet proteins in the 15–20-kDa range (Driscoll et al., 1990a; Fairbrother et al., 1991; Clubb et al.,1991). In this paper, we present the near complete ^{1}H, ^{15}N, ^{13}C, and ^{13}CO assignments of the spectrum of IL-4 using a whole array of 3D double- and triple-resonance experiments (Ikura et al., 1990a; Clore & Gronenborn, 1991b,c; Bax, 1991) to correlate ^{1}H, ^{15}N, ^{13}C, and ^{13}CO chemical shifts by means of large intra- and sequential interresidue heteronuclear scalar couplings. While this paper was being prepared for publication, a preliminary set of ^{15}N and ^{1}H backbone assignments, as well as ^{1}H assignments for 32 side chains, were reported in the literature by Redfield et al. (1991) using 3D ^{15}N-edited NMR in combination with conventinal 2D ^{1}H–^{1}H correlation spectroscopy.

EXPERIMENTAL PROCEDURES

Sample Preparation. Human recombinant IL-4 was expressed in a yeast α-factor vector expression system as described previously (Park et al., 1987). The version of IL-4 used included the addition of Glu-Ala-Glu-Ala to the N-terminus. In this paper, residues are numbered from the N-terminal Glu as residue 1, so that the natural sequence starts at residue 5. The two potential N-linked glycosylation sites at Asn 42 and Asn 109 were changed to Asp by site-directed mutagenesis (Walder & Walder, 1986) to prevent hyperglycosylation in the yeast host (Curtis et al., 1991).

Unlabeled, ^{15}N-labeled, and $^{15}N/^{13}C$-labeled human IL-4 were expressed in yeast *Saccharomyces cerevisiae* XV2181:pIXY157. The unlabeled protein was prepared in a manner similar to that described by Price et al. (1987). Single- and double-labeled proteins were prepared using a fed-batch fermentation protocol in the following manner. The inoculum was prepared in a tryptophan prototrophy selective medium using unlabeled reagents. The seed flask was grown for 24 h at 30 °C. A 1-L LH fermentor (650-mL working volume) was charged with a complex medium based on the complex enriched medium described by Fieschko et al. (1987). This medium contained either ^{15}N or $^{13}C/^{15}N$ Celtone (Martek Corp., Columbia, MD) in place of the hydrolyzed casamino acids. Celtone was batched into the fermentor to a final concentration of 5 g/L. The initial concentration of glucose in the fermentor was 5 g/L. $^{15}NH_4Cl$ (Cambridge Isotope Laboratories) and [$^{13}C_6$]glucose (Merck Isotopes) were substituted for the unlabeled species. The fermentor was maintained at pH 5.5, 30 °C, agitation rate of 1200 rpm, and an air flow of 0.5 L/min. The fermentor was charged with a 1% inoculum of the seed. After 3 h, the feed, a complex enriched medium based on the feed described by Fieschko et al. (1987) which included 50 g of Celtone/L and 220 g of glucose/L, was initiated at a rate of 0.06 mL/min. This feed rate was maintained throughout the remainder of the 48-h fermentation. Typical dry cell weight at the end of the fermentation was 45

Table I: Isotopic Label Incorporation in IL-4 Expressed in Yeast As Determined by Plasma Desorption Mass Spectrometry[a]

sample	expected mass[b]	determined mass[c]	% incorp[d]
unlabeled IL-4	15 356.8	15 354.9	
^{15}N-labeled IL-4	15 550.8	15 544.1	96.6
$^{15}N/^{13}C$-labeled IL-4	16 219.8	16 190.8	96.6

[a] Plasma desorption mass spectrometry was performed on a Bio-Ion model 20 mass analyzer using 10 μg of purified homogeneous protein evaporated to dryness, resuspended in 5 μL of 50:50 (v/v) 0.1% trifluoroacetic acid (TFA) in water/ethanol and spotted onto a nitrocellulose-coated target. The target was air-dried, washed with three 250-μL aliquots of 0.1% TFA in water, dried under nitrogen, and then placed into the instrument for analysis. Spectra were collected for 5 × 10^6 desorption events at an acceleration voltage of 15 kV. m/z was calibrated using H^+ and NO^+ ions. [b] Expected mass [in atomic mass units (amu)] was calculated from the predicted amino acid sequence for Glu-Ala-Glu-Ala-IL-4. For ^{15}N-labeled protein, the theoretical expected mass is 194 amu higher due to 194 nitrogen atoms in the sequence. For $^{13}C/^{15}N$-labeled protein, the theoretical mass is 863 amu higher due to 194 nitrogen atoms and 669 carbon atoms in the sequence. [c] Determined mass is calculated from the average of the (M + 2H)$^{2+}$, (M + 3H)$^{3+}$, and (M + 4H)$^{4+}$ ions. Little or no signal was obtained from the (M + H)$^{1+}$ ion. [d] Indicates the percent of the label incorporated versus maximum label expected.

g/L. The cells were removed by centrifugation, and the supernatant was sterile filtered (0.22 μm) prior to purification.

Recombinant protein was purified to homogeneity as determined by SDS–PAGE, N-terminal sequencing, and mass spectrometry utilizing the protocol described previously (Park et al., 1987). The same purification protocol was followed for unlabeled, ^{15}N-labeled, and $^{13}C/^{15}N$-labeled protein. Plasma desorption mass spectrometry was performed on a Bio-Ion model 20 mass analyzer. For the unlabeled protein, the purified IL-4 yielded a molecular ion determined by plasma desorption mass spectrometry that agreed with the predicted amino acid sequence, indicating that no glycosylation or other posttranslational modification was present (Table I). Molecular ion values were obtained for the labeled proteins as indicated in Table I, showing that isotopic labeling was accomplished to near theoretical maximum values. To our knowledge this is the first description of isotopic labeling of protein expressed in yeast.

Samples for NMR spectroscopy contained 2 mM protein, pH 5.7, dissolved in either 99.996% D_2O or 90% $H_2O/10\%$ D_2O.

NMR Spectroscopy. All NMR spectra were recorded at 36 °C on a Bruker AM600 spectrometer equipped with a triple-resonance ^{1}H, ^{15}N, ^{13}C probe and modified with additional hardware consisting of synthesizers, amplifiers, and fast switching devices for the third and fourth channels. The HNCO and HNCA experiments were recorded as described by Kay et al. (1990a), the HN(CO)CA experiment as described by Ikura and Bax (1991), the H(CA)NH experiment as described by Kay et al. (1990b), the HCACO and HCA-(CO)N experiments as described by Powers et al. (1991a), the HNHB experiment as described by Archer et al. (1991), the HN(CO)HB experiment as described by Grzesiek et al. (1992), the HCCH-COSY and TOCSY experiments as described by Bax et al. (1990a,b) and Clore et al. (1990), the ^{15}N-edited HOHAHA as described by Clore et al. (1991a), the ^{15}N-edited NOESY as described by Marion et al. (1989b), and the ^{13}C-edited NOESY as described by Ikura et al. (1990b). The HCACO, HCA(CO)N, HCCH-COSY, HCCH-TOCSY, and ^{13}C-edited NOESY spectra were recorded in D_2O, while all the other spectra were recorded in 90% $H_2O/10\%$ D_2O. For spectra recorded in H_2O, water suppression was achieved either by presaturation, in the case

of the HNCO, HNCA, HN(CO)CA, HNHB, and HN(CO)HB experiments, or by the use of spin-lock pulses to randomize magnetization of protons not attached to ^{15}N (Messerle et al., 1989) in the case of the H(CA)NH and ^{15}N-edited HOHAHA and NOESY experiments. Quadrature detection in the indirectly detected dimensions was obtained in all cases using the TPPI–States method (Marion et al., 1989c).

In the case of the HNCO, HNCA, HN(CO)CA, and H(CA)NH experiments, the spectral widths in the indirectly detected ^{15}N, ^{13}C, and ^{13}CO dimensions were 30.01, 33.13, and 12.05 ppm, respectively, with the carrier positions at 115, 56, and 177 ppm, respectively, and the spectral width in the ^{1}H acquisition dimension was 13.44 ppm with the carrier at the water frequency of 4.67 ppm. In the case of the ^{15}N-edited HOHAHA (mixing time 44.6 ms), ^{15}N-edited NOESY (mixing time 120 ms), and HNHB experiments, the spectral widths in the indirectly detected ^{1}H and ^{15}N dimensions were 11.4 and 30.01 ppm, respectively, with the carrier positions at 4.67 and 115 ppm, respectively, and the spectral width in the acquisition dimension was 13.44 ppm with the carrier at 4.67 ppm. The same conditions were also used for the HN(CO)HB experiment except that the spectral width in the indirectly detected ^{1}H dimension was 8.33 ppm.

For the HCACO and HCA(CO)N experiments, the spectral widths in the indirectly detected ^{13}C, ^{13}CO, and ^{15}N dimensions were 33.13, 12.05, and 30.01 ppm, respectively, with the carrier positions at 115, 56, and 175 ppm, respectively, and the spectral width in the ^{1}H acquisition dimension was 8.33 ppm with the carrier at 4.67 ppm. For the HCCH-COSY experiments, the spectral widths in the indirectly detected ^{1}H and ^{13}C dimensions were 5.95 and 20.71 ppm, respectively, with the carrier positions at 2.61 and 43 ppm, respectively, and the spectral width in the ^{1}H acquisition dimension was 8.33 pm with the carrier at 2.61 ppm. For the ^{13}C-edited NOESY experiment recorded with a mixing time of 110 ms, the spectral widths in the indirectly detected ^{1}H and ^{13}C dimensions were 9.26 and 20.71 ppm, respectively, with the carrier positions at 4.3 and 63.71 ppm, respectively, and the spectral width in the ^{1}H acquisition dimension was 10.04 pm with the carrier at 4.3 ppm.

For the HNCO, HNCA, and HN(CO)CA experiments, the number of points acquired in the various dimensions was 32 complex in F_1 (^{15}N), 64 complex in F_2 (^{13}C or ^{13}CO), and 1024 real in F_3 (^{1}H); for the HNHB experiments there were 64 complex points in F_1 (^{1}H), 32 complex points in F_2 (^{15}N), and 1024 real points in F_3 (^{1}H); for the H(CA)NH experiment there were 64 complex points in F_1 (^{1}H), 32 complex points in F_2 (^{15}N), and 1024 real points in F_3 (^{1}H); for the HN(CO)HB experiment there were 64 complex points in F_1 (^{1}H), 36 complex points in F_2 (^{15}N), and 1024 real points in F_3 (^{1}H); for the ^{15}N-edited HOHAHA and ^{15}N-edited NOESY there were 128 complex points in F_1 (^{1}H), 32 complex points in F_2 (^{15}N), and 1024 real points in F_3 (^{1}H); for the HCACO and HCA(CO)N experiments there were 32 complex points in F_1 (^{13}C), 64 complex points in F_2 (^{13}CO or ^{15}N), and 512 real in F_3; and for the HCCH-COSY, HCCH-TOCSY, and ^{13}C-edited NOESY experiments there were 128 complex points in F_1 (^{1}H), 32 complex points in F_2 (^{13}C), and 512 real points in F_3. One zero-filling was used in all dimensions, and, in the case of the HCACO and HCA(CO)N experiments, linear prediction by mean of the mirror image technique (Zhu & Bax, 1990) was used to further extend the data in the F_1 (^{13}C$^\alpha$) dimension (Powers et al., 1991a). Thus, for example, the final absorptive part of the HNCO, HN(CO)CA, and HNCA experiments consisted of 64 × 128 × 1024 points,

Table II: Summary of Correlations Observed in the 3D Double- and Triple-Resonance Experiments Used for Sequential and Side-Chain Assignments

experiment	correlation	J coupling[a]
^{15}N-edited HOHAHA	C$^\alpha$H(i)–^{15}N(i)–NH(i)	$^3J_{NH\alpha}$ (~3–11 Hz)
	C$^\beta$H(i)–^{15}N(i)–NH(i)	$^3J_{HN\alpha}$ (~3–11 Hz) and $^3J_{\alpha\beta}$ (~3–11 Hz)
H(CA)NH	C$^\alpha$H(i)–^{15}N(i)–NH(i)	$^1J_{NC\alpha}$ (~9–13 Hz)[b]
	C$^\alpha$H(i-1)–^{15}N(i)–NH(i)	$^2J_{NC\alpha}$ (~5–10 Hz)[b]
NH(CO)HB	C$^\alpha$H(i-1)–^{15}N(i)–NH(i)	$^2J_{COH\alpha}$ (~4–7 Hz)
	C$^\beta$H(i-1)–^{15}N(i)–NH(i)	$^3J_{COH\beta}$ (~8 Hz for trans coupling)
HNHB	C$^\beta$H(i)–^{15}N(i)–NH(i)	$^3J_{NH\beta}$ (~5 Hz for trans coupling)
HNCA	^{13}C$^\alpha$(i)–^{15}N(i)–NH(i)	$^1J_{NC\alpha}$ (~9–13 Hz)[b]
	^{13}C$^\alpha$(i-1)–^{15}N(i)–NH(i)	$^2J_{NC\alpha}$ (~5–10 Hz)[b]
HN(CO)CA	^{13}C$^\alpha$(i-1)–^{15}N(i)–NH(i)	$^1J_{NCO}$ (~15 Hz) and $^1J_{C\alpha CO}$ (~55 Hz)
HNCO	^{13}CO(i-1)–^{15}N(i)–NH(i)	$^1J_{NCO}$ (~15 Hz)
HCACO	C$^\alpha$H(i)–^{13}C$^\alpha$(i)–^{13}CO(i)	$^1J_{C\alpha CO}$ (~55 Hz)
HCA(CO)N	C$^\alpha$H(i)–^{13}C$^\alpha$(i)–^{15}N(i+1)	$^1J_{C\alpha CO}$ (~55 Hz) and $^1J_{NCO}$ (~15 Hz)
HCCH-COSY	H(j)–^{13}C(j)–^{13}C(j±1)–H(j±1)	$^1J_{CC}$ (~30–40 Hz)
HCCH-TOCSY	H(j)–^{13}C(j)···^{13}C(j±n)–H(j±n)	$^1J_{CC}$ (~30–40 Hz)

[a] In addition to the couplings indicated, all the experiments make use of the $^1J_{CH}$ (~140 Hz) and/or $^1J_{NH}$ (~95 Hz) couplings. [b] From Delaglio et al. (1991).

while that for the HCACO and HCA(CO)N experiments consisted of 128 × 128 × 512 points.

All spectra were processed on a Sun Sparc Workstation using in-house routines for Fourier transformation (Kay et al., 1989) and linear prediction (Zhu & Bax, 1990), together with the commercially available software package NMR2 (New Methods Research, Inc., Syracuse, NY). Analysis of the 3D spectra and peak picking was carried out using the in-house programs CAPP and PIPP (Garrett et al., 1991) and PEAK-SORT (R.P., unpublished), which are available from the authors upon request.

RESULTS AND DISCUSSION

General Assignment Strategy. Conventional sequential assignment makes use of COSY and HOHAHA spectroscopy to delineate spin systems by means of through-bond connectivities, followed by NOESY spectroscopy to identify NH(i)–NH(i+1), C$^\alpha$H(i)–NH(i+1,2,3,4), C$^\beta$H(i)–NH(i+1), and C$^\alpha$H(i)–C$^\beta$H(i+3) through-space connectivities along the polypeptide chain (Wüthrich, 1986, 1989; Clore & Gronenborn, 1987, 1989). This strategy has been applied with considerable success to proteins up to about 100 residues using 2D ^{1}H–^{1}H NMR (Dyson et al., 1990; Forman-Kay et al., 1991; Clore & Gronenborn, 1991a). For larger proteins, however, the extent of resonance overlap is such that it is necessary to increase the spectral resolution by extending the dimensionality to a third dimension (Oschkinat et al., 1988; Vuister et al., 1988; Fesik & Zuiderweg, 1988; Marion et al., 1989a,b; Kay et al., 1990b; Clore et al., 1991b; Clore & Gronenborn, 1991c). The conventional sequential assignment
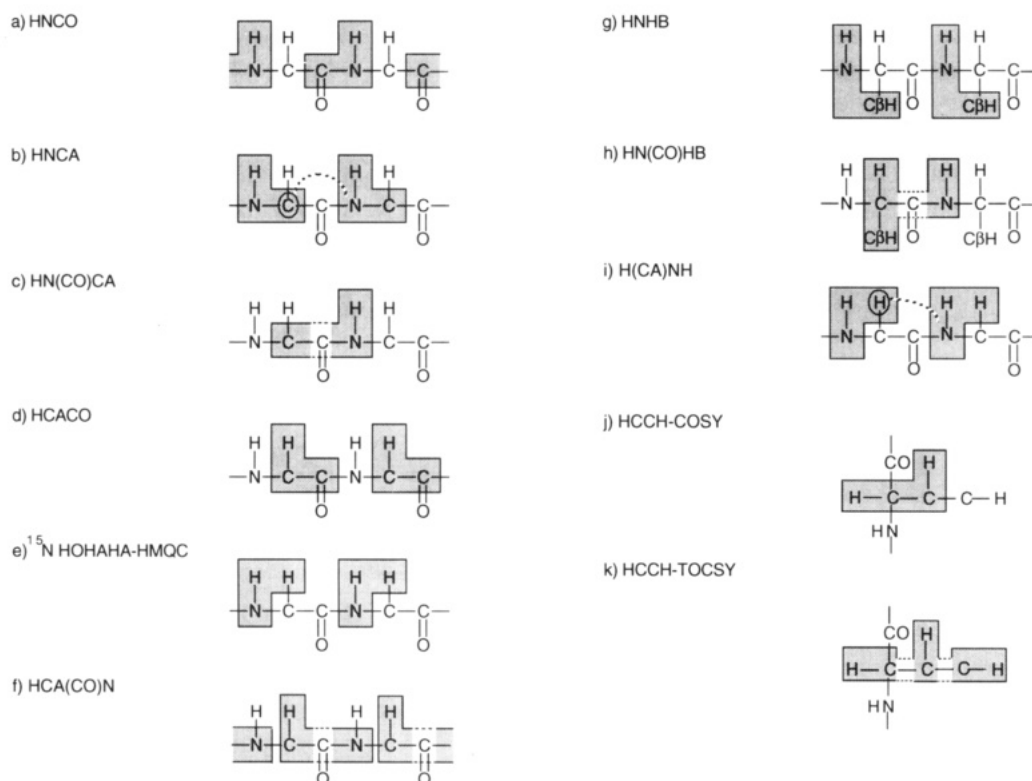
FIGURE 1: Summary of the correlations and connectivities observed in the 3D double- and triple-resonance NMR experiments used to assign the spectrum of IL-4.
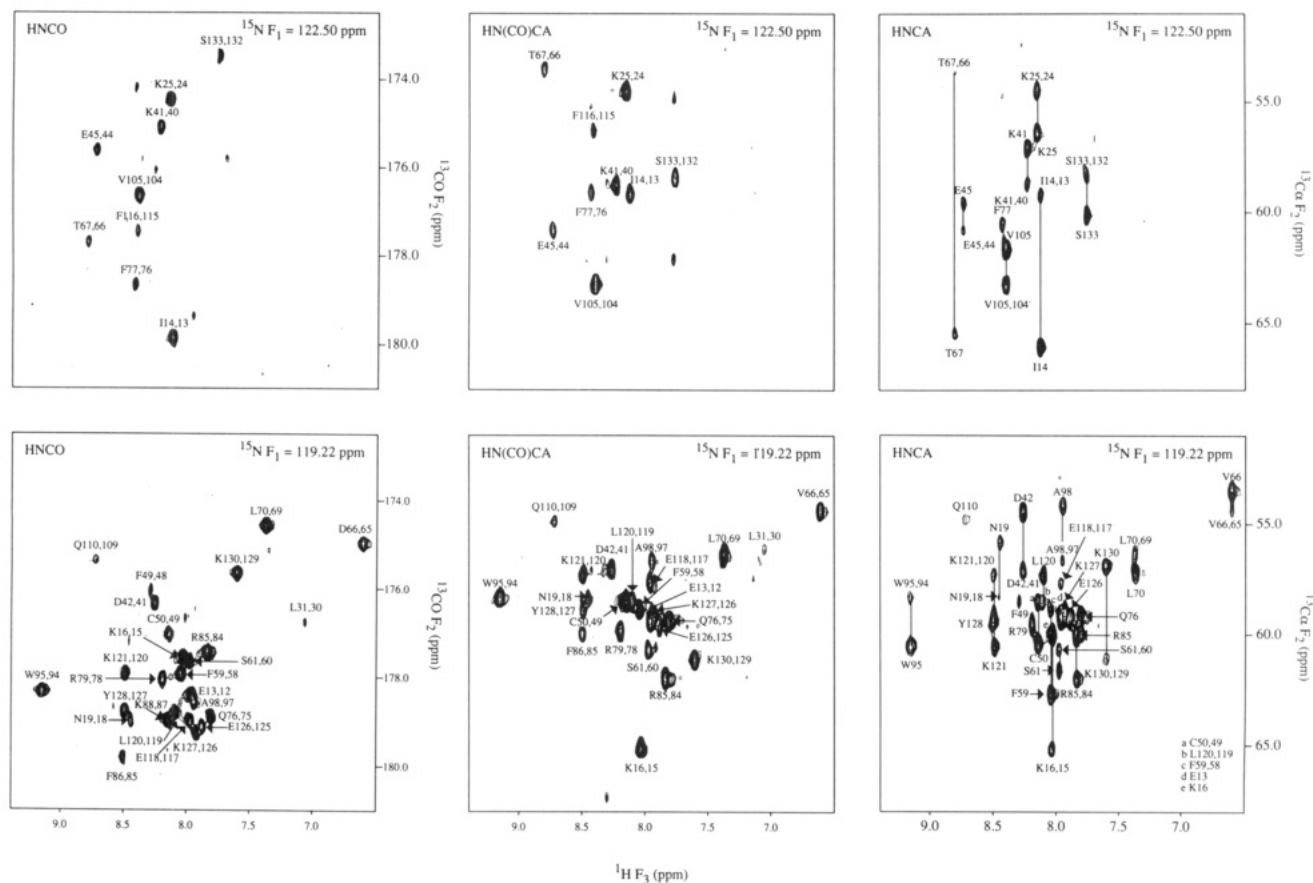
FIGURE 2: Selected $^{13}C^{\alpha}/^{13}CO(F_2)-^1H(F_3)$ planes at two different $^{15}N(F_2)$ chemical shifts of the HNCO, HN(CO)CA, and HNCA spectra of IL-4. The plane at $\delta^{15}N(F_2) = 119.22$ ppm represents one of the most crowded in the spectrum.

procedure can still be readily applied using 3D ^{15}N-edited HOHAHA and NOESY spectroscopy to identify through-bond and through-space connectivities, respectively, involving

the NH protons (Marion et al., 1989b; Driscoll et al., 1990a). The resulting spectra are similar in appearance to their 2D counterparts with the obvious difference that the various in-
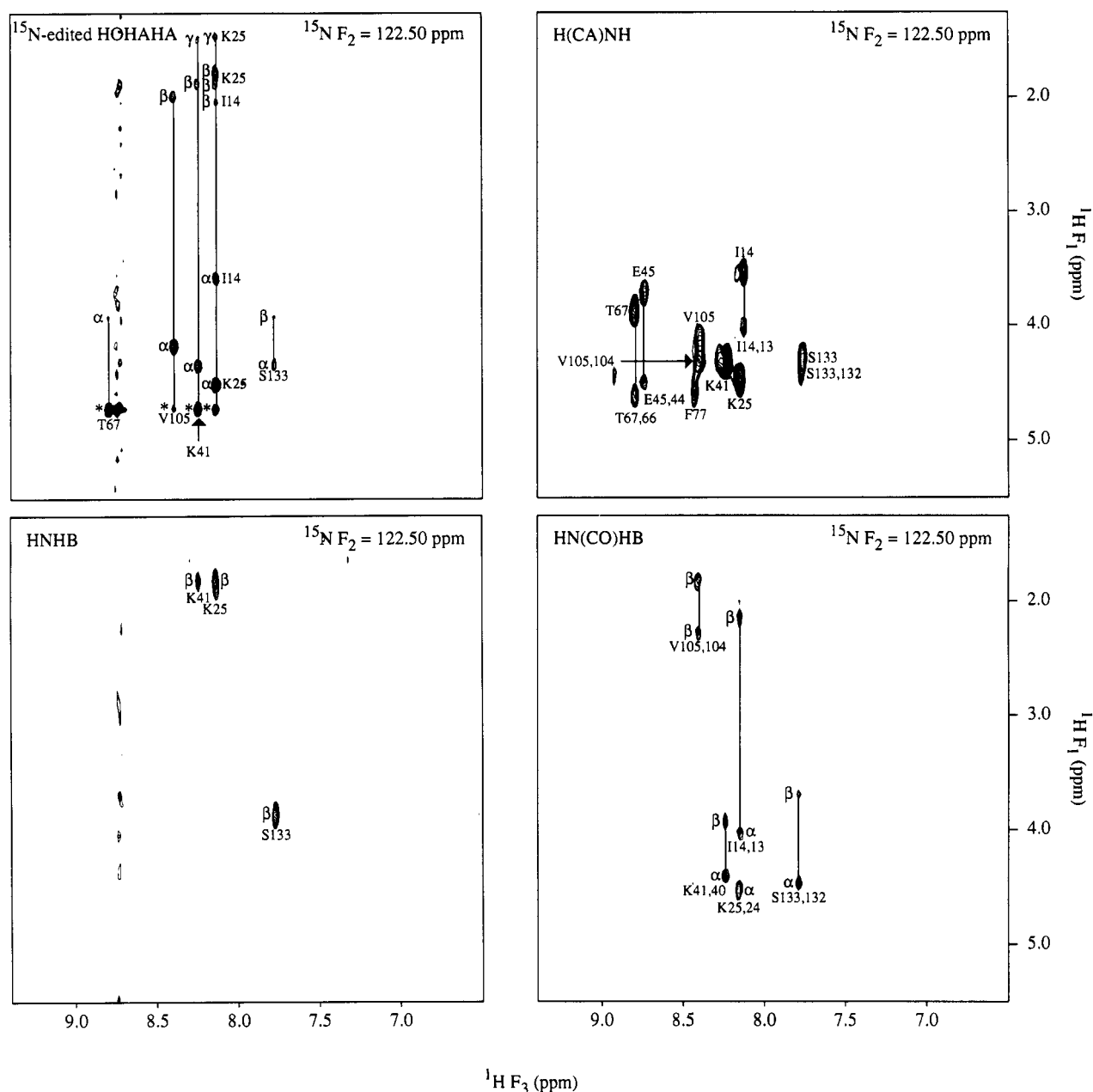
FIGURE 3A: Selected $^1H(F_1)-^1H(F_3)$ planes at $\delta^{15}N(F_2) = 122.50$ ppm of the ^{15}N-edited HOHAHA, H(CA)NH, HN(CO)HB, and HNHB spectra of IL-4. The two planes are at the same ^{15}N chemical shifts as those of the HNCO and HNCA spectra shown in Figure 2.

teractions are labeled in a third dimension according to the chemical shift of the directly bonded ^{15}N atoms. This approach was first applied successfully to interleukin-1β (153 residues; Driscoll et al., 1990a,b) and has subsequently been applied to two other proteins, *Bacillus subtilis* enzyme III^{glc} (162 residues; Fairbrother et al., 1991) and *Anacystis nidulans* flavodoxin (169 residues; Clubb et al., 1991). All three proteins, however, possess a significant amount of β-sheet structure so that the chemical shift dispersion of their ^1H spectrum is still reasonably good. For α-helical proteins, on the other hand, the overall ^1H chemical shift dispersion tends to be very poor, and there is usually extensive chemical shift degeneracy. As a result, sequential assignment relying on ^{15}N-edited spectroscopy, complemented by the appropriate 2D experiments, rapidly breaks down. To circumvent this problem, an alternative approach has been suggested which relies entirely on heteronuclear scalar couplings to obtain sequential connectivities along the chain by means of various combinations of ^1H, ^{15}N, ^{13}C, and ^{13}CO correlations (Ikura et al., 1990a).

The original strategy based on heteronuclear scalar couplings relied on four triple-resonance experiments and one-double resonance experiment and has been successfully applied to three proteins, calmodulin (Ikura et al., 1990, 1991), the RNase H domain of HIV-1 reverse transcriptase (Powers et al., 1991b), and *Escherichia coli* enzyme III^{glc} (Pelton et al., 1991). Specifically NH(i)–^{15}N(i)–^{13}CO(i–1), NH(i)–^{15}N(i)–$^{13}C^\alpha$(i,i–1), and NH(i)–^{15}N(i)–C^αH(i) correlations were established from HNCO, HNCA, and ^{15}N-edited HOHAHA spectra recorded in H_2O, while C^αH(i)–$^{13}C^\alpha$(i)–^{13}CO(i) and C^αH(i)–$^{13}C^\alpha$(i)–^{15}N(i+1) correlations were obtained from HCACO and HCA(CO)N spectra recorded in D_2O. In these proteins the resolution afforded by these experiments was sufficient to obtain complete backbone assignments with only minimal reference to side-chain spin system identification. In the case of IL-4, on the other hand, there were sufficient ambiguities still present in these spectra to necessitate rigorous spin system identification. This was carried out using the HCCH-COSY and HCCH-TOCSY experiments to obtain
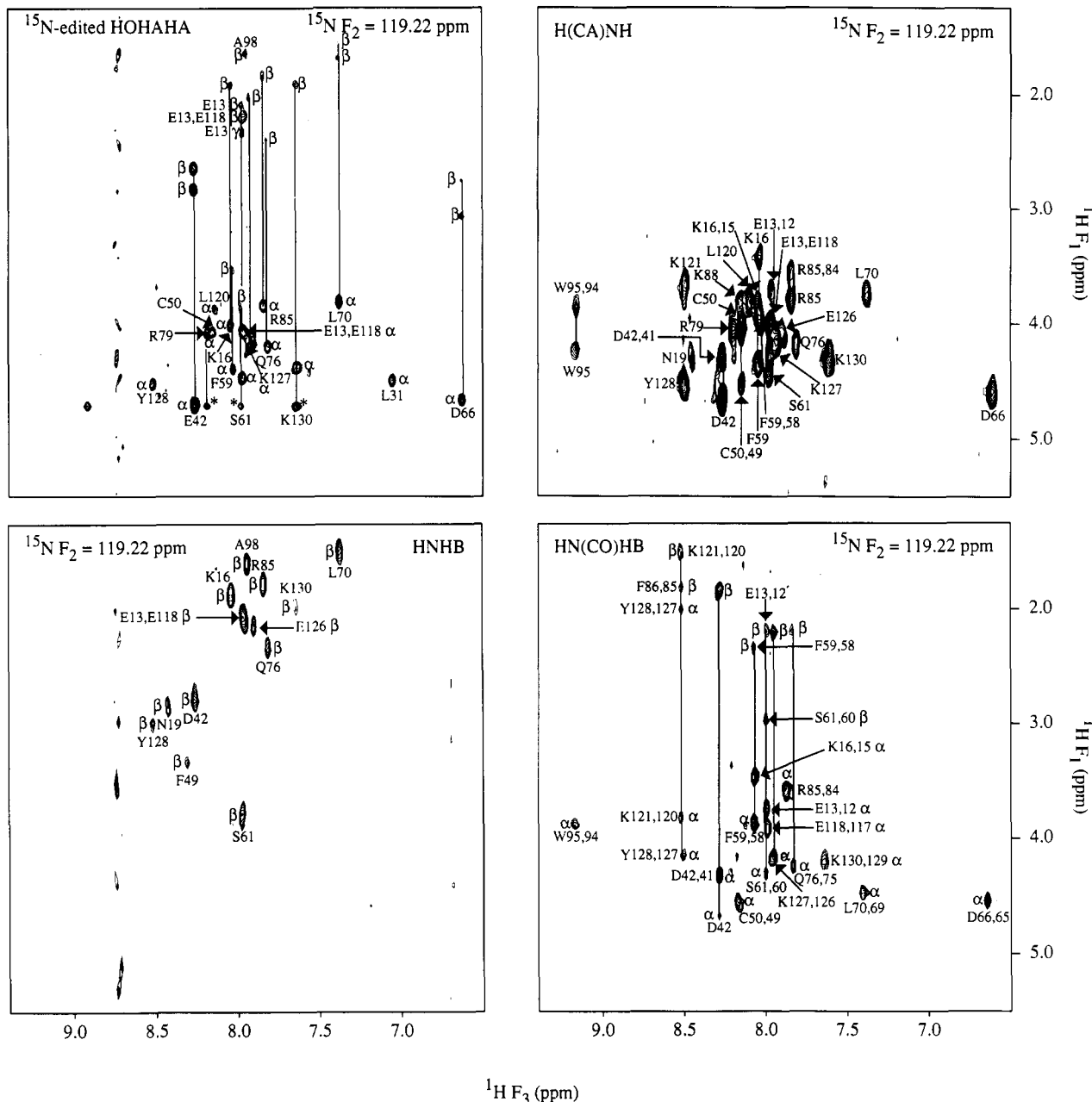
FIGURE 3B: Selected $^1H(F_1)-^1H(F_3)$ planes at $\delta^{15}N(F_2) = 119.22$ ppm of the ^{15}N-edited HOHAHA, H(CA)NH, HN(CO)HB, and HNHB spectra of IL-4. The two planes are at the same ^{15}N chemical shifts as those of the HNCO and HNCA spectra shown in Figure 2.

$^1H-^{13}C-^1H$ scalar correlations via direct and relayed magnetization transfer, respectively, along the carbon chain. Further, a number of other triple-resonance experiments had to be interpreted to obtain unambiguous sequential assignments.

A total of 11 double- and triple-resonance 3D correlation experiments were recorded. The various correlations obtained in these experiments are summarized in Figure 1 and Table II. In the original triple-resonance assignment strategy, there were three pathways for obtaining interresidue conectivities: namely, the $^{13}C^\alpha(i-1)-^{15}N(i)-NH(i)$ correlation in the HNCA experiment via the $^2J_{NC\alpha}$ coupling, the $^{13}CO(i-1)-^{15}N(i)-NH(i)$ correlation in the HNCO experiment via the $^1J_{NCO}$ coupling, and the $C^\alpha H(i)-^{13}C^\alpha(i)-^{15}N(i+1)$ correlation via the $^1J_{C\alpha CO}$ and $^1J_{NCO}$ couplings. In the present series of experiments, two additional sequential correlations have been added. Thus, the H(CA)NH experiment provides the $C^\alpha H(i-1)-^{15}N(i)-NH(i)$ correlation via the $^2J_{NC\alpha}$ coupling, and the HN(CO)HB experiment yields the $C^\beta H(i-1)-^{15}N(i)-NH(i)$

correlation via the $^3J_{COH\beta}$ coupling, as well as a $C^\alpha H(i)-^{15}N(i)-NH(i)$ correlation via the $^2J_{COH\alpha}$ coupling. In addition, an alternative pathway for the $^{13}C^\alpha(i-1)-^{15}N(i)-NH(i)$ correlation is provided by the HN(CO)CA experiment through the $^1J_{NCO}$ and $^1J_{CACO}$ couplings. The latter experiment is particularly useful, as its sensitivity for demonstrating $^{13}C^\alpha(i-1)-^{15}N(i)-NH(i)$ correlations is considerably higher than that of the HNCA experiment owing to the fact that the one-bond couplings ($^1J_{NCO}$ and $^1J_{C\alpha CO}$) are significantly larger than the two-bond coupling ($^2J_{NC\alpha}$) employed in the HNCA experiment. Further, as only a single correlation is observed in the HN(CO)CA experiment, any potential ambiguity in distinguishing between the intraresidue and interresidue correlation observed in HNCA experiment can be resolved. Although the relative intensities of the latter may serve as a yardstick, the intraresidue cross-peaks generally being stronger than the corresponding interresidue ones (Ikura et al., 1990a; Clore & Gronenborn, 1991b), there are cases where the relative intensities are either very similar or actually reversed,
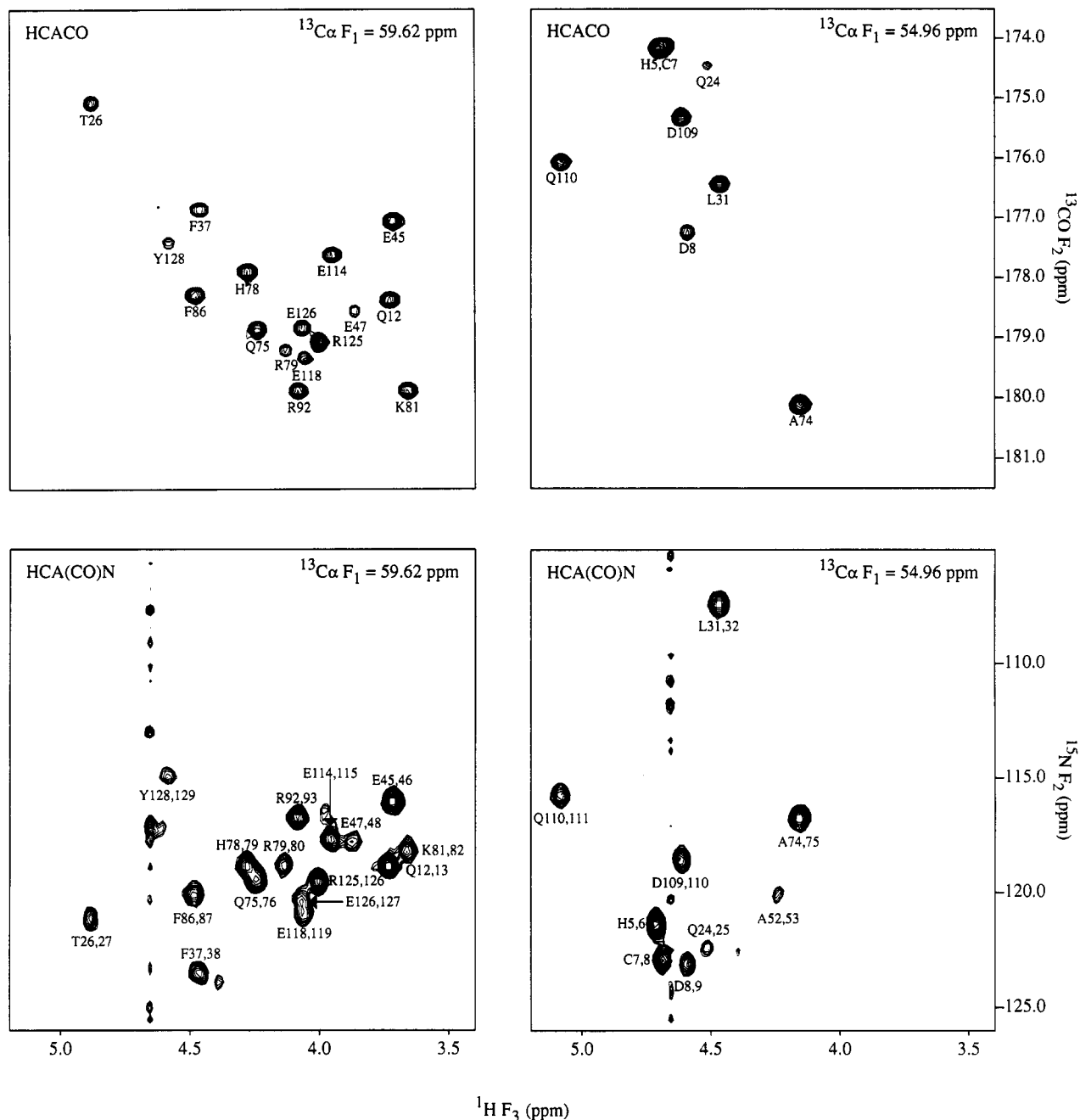
FIGURE 4: Selected ^{15}N/^{13}CO(F_2)–^{1}H(F_3) planes at two different ^{13}C$^\alpha$(F_1) chemical shifts of the HCACO and HCA(CO)N spectra of IL-4.

creating difficulties in interpretation (Powers et al., 1991b). Equally important in the triple-resonance assignment strategy is the identification of backbone intraresidue connectivities. In the original set of experiments, there were three intraresidue correlations: the C$^\alpha$H(i)–^{15}N(i)–NH(i) correlation from the ^{15}N-edited HOHAHA experiment via the $^3J_{HN\alpha}$ coupling, the ^{13}C$^\alpha$(i)–^{15}N(i)–NH(i) correlation in the HNCA experiment via the $^1J_{NC\alpha}$ coupling, and the C$^\alpha$H(i)–^{13}C$^\alpha$(i)–^{13}CO(i) correlation in the HCACO experiment via the $^1J_{C\alpha CO}$ coupling. In the present scheme, the C$^\alpha$H(i)–^{15}N(i)–NH(i) correlation is also obtained from the H(CA)NH experiment via the $^1J_{NC\alpha}$ coupling. For helical proteins, this is particularly advantageous as the size of the $^1J_{NC\alpha}$ coupling (7–11 Hz) is independent of secondary structure, whereas the $^3J_{HN\alpha}$ couplings used in the ^{15}N-edited HOHAHA experiment are small in helices ($\sim$3–5 Hz), resulting in weak or no correlations at all. In addition, intraresidue C$^\beta$H(i)–^{15}N(i)–NH(i) correlations are observed in the HNHB experiment via the $^3J_{NH\beta}$ coupling under con-

ditions where the C$^\beta$H proton is trans to the nitrogen atom. C$^\beta$H(i)–^{15}N(i)–NH(i) correlations can also sometimes be observed in the ^{15}N-edited HOHAHA experiment via a two-step relayed magnetization transfer pathway involving the $^3J_{HN\alpha}$ and $^3J_{\alpha\beta}$ couplings. For larger proteins, it is usually the case that only the correlation to the C$^\beta$H proton trans to the C$^\alpha$H proton is observed in this manner, except in cases of conformational disorder about χ_1. As the C$^\beta$H proton cannot be trans to both the C$^\alpha$H proton and the nitrogen atom simultaneously, these two experiments complement each other.

IL-4 Resonance Assignments. Examples of selected planes of the 3D spectra used for the sequential assignment are shown in Figures 2–5, a summary of the sequential connectivities is given in Figure 6, and the ^{1}H, ^{15}N, ^{13}C, and ^{13}CO resonance assignments are provided in Table III. For completeness, the assignment of aromatic and amide side-chain resonances are also included. The aromatic side-chain assignments were obtained from 2D HOHAHA (Bax, 1989) and P.COSY
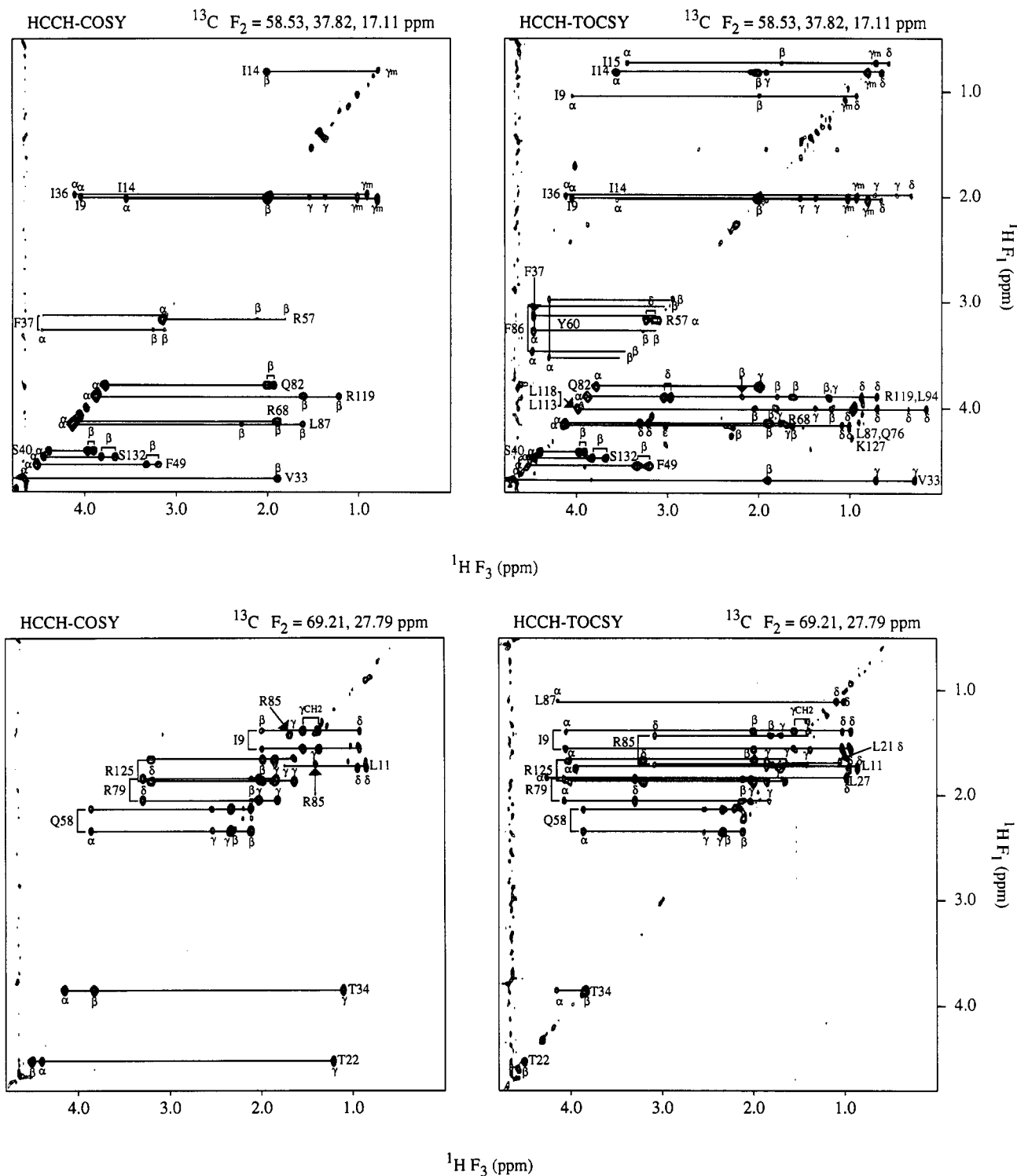
FIGURE 5: Selected $^1H(F_1)$–$^1H(F_3)$ planes at two different ^{13}C chemical shifts of the HCCH-COSY and HCCH-TOCSY spectra of IL-4. Note that extensive folding is used so that each plane corresponds to several ^{13}C chemical shifts with a separation of 20.71 ppm. (A, top) $\delta^{13}C(F_2)$ 58.53, 37.82, 17.11 ppm; (B, bottom) $\delta^{13}C(F_2)$ = 69.21, 27.79 ppm.

(Marion & Bax, 1988) spectra and assigned to specific residues from the observation of intraresidue NOEs from the aromatic ring protons ($C^\delta H$ of Phe and Tyr, $C^{\delta 2}H$ of His, and $C^{\delta 1}H$ and $C^{\epsilon 3}H$ of Trp) to the $C^\alpha H$ and $C^\beta H$ protons in a 3D ^{13}C-edited NOESY spectrum (data not shown). Similarly, the amide side-chain assignments of Asn and Gln were obtained from a 2D ^1H–^{15}N Overbodenhausen correlation spectrum (Bax et al., 1990c; Norwood et al., 1990) and assigned to specific residues from the observation of intraresidue NOEs from the NH_2 protons to the $C^\beta H$ and $C^\gamma H$ protons, respectively, in a 3D ^{15}N-edited NOESY spectrum.

Semiautomated Sequential Assignment of IL-4. The large number of 3D spectra recorded generates a huge amount of data such that data analysis by traditional manual methods employing paper plots becomes almost impossible. For this reason we developed a semiautomated protocol which permitted us to obtain the complete assignments within a relatively short period of time (approximately 2–3 weeks) once all the 3D double- and triple-resonance spectra had been recorded and processed.

The semiautomatic protocol makes use of the programs CAPP (contour approach to peak picking), PIPP (primitive interactive

```
 1    5      10       15      20        25        30       35      40       45       50        55      60        65
EAEAHKCD I TLQE I IKTLNSLTEQKTLCTEL TVTD I FAASKDTTEKETFCRAATVLRQFYSHHEKDT
```



```
         70       75      80       85       90       95      100      105      110      115      120      125      130
         RCLGATAQQFHRHKQL I RFLKRLDRNLWGLAGLNSCPVKEADQSTLENFLERLKT IMREKYSKCSS
```


FIGURE 6: Summary of the sequential scalar connectivities observed in the 3D triple-resonance experiments for IL-4. The $CO(i)-N(i+1),NH(i+1)$ correlations are observed in the HNCO spectrum, the $C^\alpha H(i),C^\alpha(i)-N(i+1)$ correlations in the HCA(CO)N spectrum, the $C^\alpha(i)-N(i+1),NH(i+1)$ correlations in the HNCA and HN(CO)CA spectra, the $C^\alpha H(i)-N(i+1),NH(i+1)$ correlations in the H(CA)NH and HN(CO)HB spectra, and the $C^\beta H(i)-N(i+1),NH(i+1)$ correlations in the HN(CO)HB spectrum.

peak picker), and PEAK-SORT developed in our laboratory (Garrett et al., 1991; R.P., unpublished results). The procedure first involves automatically peak-picking the various triple-resonance experiments using the program CAPP. This program models the contour diagrams from the 3D data sets as a series of ellipses and determines the position of a given real peak when the simulated ellipse meets four conditions: namely, (i) the RMS deviation between contour points and the ellipse must be less than a predetermined cutoff value; (ii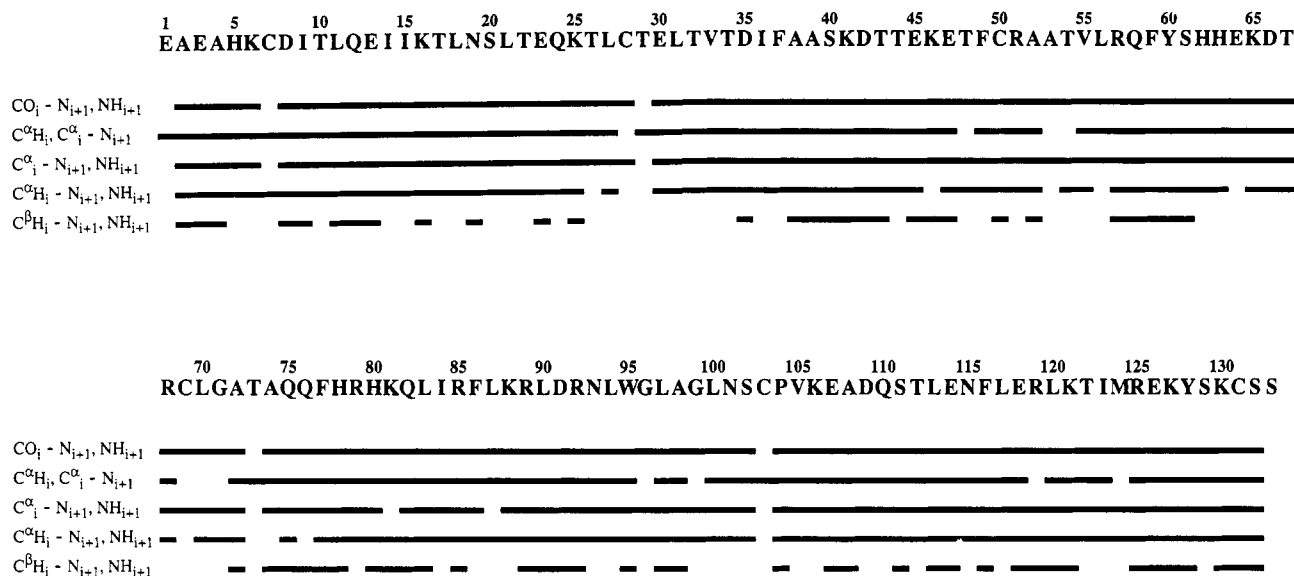) the radius of the ellipse along each axis must lie within defined limits; (iii) the ratio of the ellipse radii must be between defined limits; and finally (iv) the percentage circumference deviation between the ellipse and the contour must be less than a cutoff value. This procedure yields an efficiency of 75–90% in terms of correctly peak-picking the triple-resonance 3D data. The interactive peak-picker program PIPP is then used to manually refine the peak table generated by CAPP by adding peaks missed by CAPP and/or removing incorrectly assigned peaks (i.e., peaks due to artifacts such as t_1 noise). The next step involves correlating the intraresidue connectivities observed in the various triple-resonance experiments on the basis of the table of peak coordinates generated by CAPP and PIPP. This is accomplished with the program PEAK-SORT, which compares information in common between any two experiments, determines a best fit of the chemical shifts based on an upper-limit cutoff and the RMS difference, and appends the new correlated data into a sorted peak table. For example, a comparison of the HNCO and HNCA experiments is based on the common ^{15}N and NH chemical shifts. PEAK-SORT will locate common pairs of ^{15}N and NH chemical shifts between the two experiment and create a file containing the ^{15}N, NH, $^{13}C^\alpha$, $^{13}C^\alpha(i-1)$, and $^{13}CO(i-1)$ chemical shifts. The program fails when there is any degeneracy, requiring a manual analysis of such regions and appropriate correction of the sorted peak table. Once all the intraresidue connectivities have been appropriately correlated by this means, PEAK-SORT makes use of the interresidue connectivities [i.e., $C^\alpha H(i-1)$, $C^\beta H(i-1)$, $C^\alpha(i-1)$, $CO(i-1)$, $NH(i+1)$] associated with each residue in the peak table to locate its $i-1$ residue on the basis of a RMS best fit of the interresidue and intraresidue connectivities. The program then attempts to link together the $(i,i-1)$ assigned

pairs on the basis of identity (ID) numbers to form a sequential chain. For example, the two assigned pairs 2_{i-1}, 11_i and 11_{i-1}, 3_i will be linked to form the sequential chain 2–11–3. In theory, the PEAK-SORT program could generate a continuous sequential connectivity chain corresponding to the complete backbone assignments. In practice, however, it generates a good starting point for manually completing the sequential assignments. Difficulties arise from chemical shift degeneracy which may result in incorrect correlation of data between the various triple-resonance experiments and from missing cross-peaks in the triple-resonance spectra. These problems can cause both termination of sequential assignment chains and incorrect sequential assignments. At the present time, these problems can only be overcome by manually cross-checking the data.

In the case of IL-4, the 3D triple-resonance spectra exhibited a high degree of peak overlap and degeneracy owing to the high α-helical content of this protein and the absence of any significant degree of β-sheet structure. This was particularly true of the ^{15}N and NH chemical shifts. For example, Figures 2 and 3 illustrates two sets of $F_1(^{13}C^\alpha/^{13}CO/^1H)-F_3(NH)$ planes of the HNCA, HN(CO)CA, and HNCO spectra and the ^{15}N-edited HOHAHA, H(CA)NH, HN(CO)HB, and HNHB spectra, respectively, corresponding to $^{15}N(F_2)$ chemical shifts of 119.22 and 122.50 ppm. The planes at $\delta^{15}N(F_2)$ = 122.50 ppm demonstrates a fairly typical 3D triple-resonance slice containing a modest number of well-resolved cross-peaks corresponding to a handful of residues. Thus, establishing the various correlations and connectivities from such a set of planes is a simple matter. In contrast, the planes at $\delta^{15}N(F_2)$ = 119.22 ppm are extremely crowded with extensive overlap in the NH dimension. In particular, Glu-13, Ser-61, and Glu-118 have degenerate NH chemical shifts at 7.96 ppm and are nearly degenerate with Ala-98; similarly, the NH resonances of Lys-16, Phe-86, Lys-121, and Tyr-128 are nearly degenerate at 8.5 ppm.

Fortunately, the chemical shift dispersion afforded in the $^{13}C^\alpha-^1H$ dimensions was significantly better than that in the ^{15}N-NH dimensions. This can clearly be seen in Figure 4, which illustrates two sets of $F_2(^{13}CO/^{15}N)-F_3(^1H)$ planes from the HCACO and HCA(CO)N experiments taken at $^{13}C^\alpha(F_1)$

Table III: ^{15}N, ^{13}C, ^{13}CO, and ^1H Resonance Assignments for IL-4 at pH 5.7 and 36 °C[a]

residue	N	CO	C^α	C^β	others
E1	–	172.3	55.4 (4.08)	30.1 (2.15)	C^γ 34.0 (2.42)
A2	125.5 (–)	177.2	52.5 (4.38)	18.6 (1.42)	
E3	120.7 (8.47)	176.1	56.5 (4.25)	30.1 (2.01, 1.95)	C^γ 36.1 (2.29)
A4	124.8 (8.27)	177.4	52.4 (4.30)	19.1 (1.33)	
H5	117.4 (8.41)	174.2	55.0 (4.73)	29.0 (3.31, 3.19)	$C^{\epsilon 1}$ 136.2 (8.55); $C^{\delta 2}$ 120.0 (7.29)
K6	121.6 (8.22)	176.5	56.3 (4.48)	33.2 (1.88, 1.78)	C^γ 24.6 (1.46); C^ϵ 40.8 (3.17, 2.67)
C7	120.1 (8.58)	174.2	54.9 (4.70)	41.6 (3.15, 2.98)	
D8	123.0 (8.41)	177.3	54.6 (4.62)	42.4 (2.81, 2.69)	
I9	123.3 (8.43)	177.2	63.6 (4.06)	38.1 (1.99)	C^γ 28.1 (1.54, 1.37); $C^{\gamma m}$ 17.6 (1.01); C^δ 13.3 (0.92)
T10	117.1 (8.31)	176.6	65.6 (3.99)	68.3 (4.12)	C^γ 22.3 (1.24)
L11	121.2 (7.76)	178.4	57.9 (3.96)	41.7 (1.85, 1.68)	C^γ 27.8 (1.74); C^δ 25.2 (0.94), 24.9 (0.85)
Q12	116.5 (7.86)	178.4	59.4 (3.74)	28.5 (2.17, 2.17)	C^γ 34.2 (2.42, 2.27); N^ϵ 111.1 (7.17, 6.83)
E13	118.9 (7.96)	179.9	59.1 (4.02)	29.2 (2.15, 2.06)	C^γ 35.9 (2.32, 2.27)
I14	122.2 (8.12)	177.2	66.0 (3.57)	37.8 (2.01)	C^γ 30.3 (1.91, 0.79); $C^{\gamma m}$ 17.1 (0.80); C^δ 14.5 (0.67)
I15	120.2 (7.98)	177.6	65.1 (3.46)	37.2 (1.74)	C^γ 29.5 (1.35, 0.95); $C^{\gamma m}$ 16.5 (0.71); C^δ 12.2 (0.57)
K16	119.4 (8.03)	179.7	59.9 (3.99)	32.2 (1.88, 1.88)	C^γ 25.1 (1.57, 1.41); C^δ 29.2 (1.66); C^ϵ 41.79 (2.91)
T17	116.8 (8.13)	176.2	67.1 (3.65)	67.4 (4.25)	C^γ 22.6 (1.14)
L18	121.5 (8.55)	179.0	58.3 (4.00)	41.8 (2.04, 1.19)	C^γ 27.2 (1.80); C^δ 24.6 (0.94), 26.3 (0.71)
N19	119.7 (8.45)	177.4	55.7 (4.33)	37.1 (2.94, 2.82)	N^δ 110.2 (7.48, 6.59)
S20	115.8 (7.76)	176.4	61.8 (4.26)	62.9 (3.61, 3.58)	
L21	120.3 (8.04)	178.1	57.2 (4.07)	43.7 (1.92, 1.51)	C^γ 27.5 (1.68); C^δ 25.4 (1.05), 27.1 (0.86)
T22	107.0 (7.66)	175.2	62.7 (4.41)	69.2 (4.51)	C^γ 21.8 (1.21)
E23	119.8 (7.37)	176.3	57.3 (4.28)	30.0 (2.13, 2.13)	C^γ 35.9 (2.36, 2.45)
Q24	116.9 (7.43)	174.5	54.4 (4.53)	29.8 (2.11, 1.99)	C^γ 33.2 (2.35, 2.29); N^ϵ 110.6 (7.43, 6.58)
K25	122.6 (8.14)	176.6	56.3 (4.48)	32.7 (1.85, 1.77)	C^γ 24.6 (1.38); C^δ 28.9 (1.67); C^ϵ 41.8 (3.00)
T26	114.9 (8.26)	175.1	59.7 (4.90)	71.6 (4.60)	C^γ 21.9 (1.29)
L27	121.4 (8.46)	178.7	57.6 (4.28)	42.3 (1.90, 1.69)	C^γ 27.4 (1.82); C^δ 24.9 (0.97), 23.6 (0.97)
C28	114.2 (8.42)	175.7	57.3 (4.57)	40.7 (3.63, 3.14)	
T29	107.7 (7.76)	174.0	64.3 (4.24)	67.9 (4.17)	C^γ 22.3 (1.35)
E30	117.4 (–)	176.8	55.9 (4.54)	29.5 (2.29, 2.06)	C^γ 35.9 (2.44, 2.34)
L31	118.6 (7.05)	176.5	54.9 (4.48)	41.1 (2.05, 1.62)	C^γ 27.2 (1.84); C^δ 25.2 (0.63); 21.9 (0.86)
T32	107.5 (7.77)	174.8	61.2 (5.09)	71.5 (4.22)	C^γ 21.3 (1.12)
V33	113.3 (8.98)	174.5	58.6 (4.67)	35.9 (1.89)	C^γ 23.3 (0.70); 18.4 (0.28)
T34	118.3 (7.81)	173.2	64.1 (4.16)	69.2 (3.83)	C^γ 22.6 (1.10)
D35	123.8 (8.66)	177.4	52.8 (4.72)	39.9 (2.85, 2.35)	
I36	116.6 (7.02)	176.4	61.4 (4.15)	37.6 (2.01)	C^γ 25.9 (0.72, 0.48); $C^{\gamma m}$ 21.6 (0.91); C^δ 14.9 (0.34)
F37	119.9 (8.15)	176.9	59.4 (4.48)	37.9 (3.25, 3.12)	C^δ 131.7 (7.27); C^ϵ 131.0 (6.65); C^ζ 127.9 (6.55)
A38	123.7 (7.46)	177.8	53.6 (4.26)	18.3 (1.44)	
A39	120.3 (7.68)	177.5	52.0 (4.51)	20.1 (1.40)	
S40	113.9 (7.77)	175.1	58.6 (4.41)	63.6 (3.97, 3.90)	
K41	122.7 (8.22)	176.3	56.9 (4.33)	32.4 (1.81)	C^γ 24.6 (1.44); C^δ 28.7 (1.86, 1.70); C^ϵ 41.5 (3.04)
D42	119.3 (8.26)	175.8	54.4 (4.68)	40.7 (2.79, 2.61)	
T43	114.4 (7.77)	174.6	61.4 (4.54)	70.1 (4.13)	C^γ 21.1 (1.20)
T44	114.4 (8.36)	175.6	60.7 (4.53)	71.1 (4.59)	C^γ 21.7 (1.34)
E45	122.7 (8.72)	177.1	59.5 (3.74)	29.3 (1.86, 1.86)	C^γ 36.7 (1.94, 1.86)
K46	116.1 (7.98)	178.5	60.5 (3.88)	32.1 (2.01, 1.85)	C^γ 26.0 (1.72, 1.62); C^δ 29.1 (1.85); C^ϵ 41.8 (3.12)
E47	117.7 (7.53)	178.6	59.8 (3.89)	29.5 (2.20, 1.95)	C^γ 37.2 (2.24, 2.24)
T48	117.9 (8.03)	–	67.2 (3.78)	67.6 (4.11)	C^γ 21.4 (1.11)
F49	119.8 (8.30)	177.0	58.5 (4.54)	36.9 (3.33, 3.20)	C^δ 129.8 (6.93); C^ϵ 131.1 (7.25); C^ζ 129.1 (7.08)
C50	119.2 (8.14)	177.7	60.4 (4.02)	40.7 (3.31, 3.05)	
R51	123.7 (9.01)	178.3	60.1 (3.92)	30.4 (1.98, 1.70)	C^γ 28.6 (2.10); C^δ 44.0 (3.24, 3.07)
A52	121.3 (8.80)	178.4	55.3 (4.25)	18.3 (1.67)	
A53	120.2 (8.19)	179.0	55.7 (4.04)	17.3 (1.68)	
T54	113.8 (8.18)	176.8	67.4 (3.85)	68.8 (4.58)	C^γ 21.3 (1.30)
V55	120.5 (8.24)	179.1	66.3 (3.88)	31.6 (2.26)	C^γ 22.6 (1.12), 21.6 (0.82)
L56	121.0 (8.15)	177.4	58.1 (4.04)	41.5 (2.27, 1.47)	C^γ 26.3 (2.20); C^δ 26.6 (0.97), 23.5 (0.85)
R57	120.2 (8.32)	179.9	58.4 (3.17)	29.8 (2.11, 1.80)	C^γ 25.6 (1.53, 1.34); C^δ 44.0 (3.25, 3.07)
Q58	120.6 (8.09)	178.0	58.8 (3.87)	27.9 (2.33, 2.11)	C^γ 33.6 (2.53, 2.33); N^ϵ 110.2 (7.25, 6.76)
F59	119.2 (8.04)	179.1	62.7 (4.37)	38.7 (3.49, 3.19)	C^δ 132.1 (7.15); C^ϵ 131.0 (6.99); C^ζ 118.7 (7.35)
Y60	117.1 (9.24)	177.6	60.8 (4.31)	37.7 (3.51, 2.95)	C^δ 135.0 (6.98); C^ϵ 118.3 (6.86)
S61	118.9 (7.97)	176.1	61.5 (4.46)	62.5 (3.84, 3.77)	
H62	116.4 (7.55)	176.4	56.5 (4.61)	29.5 (2.81, 2.72)	$C^{\epsilon 1}$ 136.2 (8.41); $C^{\delta 2}$ 119.3 (7.10)
H63	111.4 (7.92)	175.1	55.3 (5.08)	28.5 (3.47, 2.29)	$C^{\epsilon 1}$ 137.5 (8.50); $C^{\delta 2}$ 122.2 (6.07)
E64	124.3 (8.09)	176.9	61.2 (4.00)	28.8 (2.60, 2.15)	C^γ 36.0 (2.30, 2.30)
K65	116.3 (8.59)	174.9	54.3 (4.54)	31.5 (2.12, 1.63)	C^γ 25.1 (1.37); C^δ 29.1 (1.73); C^ϵ 41.8 (3.00)
D66	119.2 (6.61)	177.7	53.4 (4.64)	42.4 (3.02, 2.73)	
T67	122.5 (8.80)	176.7	65.3 (3.93)	68.5 (4.30)	C^γ 21.9 (1.37)
R68	121.5 (8.50)	177.6	58.5 (4.13)	29.9 (1.89)	C^γ 26.9 (1.75, 1.73); C^δ 43.3 (3.31, 3.22)
C69	113.3 (7.46)	174.6	56.5 (4.40)	– (3.11)	
L70	119.2 (7.37)	176.3	57.2 (3.79)	42.6 (1.65, 1.49)	C^γ 26.8 (1.49); C^δ 25.1 (0.76), 23.9 (0.76)
G71	99.1 (7.09)	173.8	45.2 (3.98, 3.72)		
A72	120.7 (8.40)	177.7	52.1 (4.75)	21.2 (1.48)	
T73	107.1 (7.58)	174.8	58.8 (4.75)	72.4 (4.70)	C^γ 21.4 (1.28)
A74	124.6 (–)	180.2	55.0 (4.17)	17.8 (1.50)	
Q75	117.0 (8.52)	178.9	59.3 (4.26)	28.3 (2.20, 2.10)	C^γ 34.1 (2.51, 2.51); N^ϵ 111.6 (7.53, 6.93)
Q76	119.5 (7.81)	178.7	59.1 (4.17)	28.4 (2.35, 2.35)	C^γ 34.6 (2.55, 2.55); N^ϵ 112.5 (7.56, 7.07)
F77	123.0 (8.42)	178.1	60.4 (4.61)	38.5 (3.51, 3.29)	C^δ 128.5 (7.20), C^ϵ – (7.37); C^ζ – (7.32)

Table III (Continued)

residue	N	CO	Cα	Cβ	others
H78	117.7 (8.45)	177.9	59.6 (4.30)	29.6 (3.36, 3.36)	$C^{\epsilon 1}$ 137.8 (8.14); $C^{\delta 2}$ 119.6 (7.18)
R79	118.8 (8.19)	179.2	59.5 (4.09)	– (2.12)	C^γ 27.9 (2.03, 1.82); C^δ 43.6 (3.31)
H80	120.5 (8.31)	176.8	59.8 (4.64)	30.7 (3.35, 3.24)	$C^{\epsilon 1}$ 137.5 (7.72); $C^{\delta 2}$ 117.7 (6.93)
K81	117.3 (8.13)	179.9	59.4 (3.68)	31.4 (1.86, 1.70)	C^γ 24.8 (1.42, 1.26); C^δ 28.7 (1.56); C^ϵ 41.7 (2.85, 2.74)
Q82	118.3 (7.91)	176.6	58.5 (3.79)	28.7 (2.01, 1.93)	C^γ 33.9 (1.98, 1.98); N^ϵ 111.8 (7.07, 6.81)
L83	121.5 (7.92)	178.5	58.9 (4.08)	40.8 (2.23, 1.76)	C^γ 27.5 (1.53); C^δ 25.7 (1.02), 24.2 (0.94)
I84	116.4 (8.10)	177.4	62.0 (3.60)	34.5 (2.09)	C^γ – (1.40, 1.08); $C^{\gamma m}$ 17.5 (0.79); C^δ 8.00 (0.74)
R85	119.2 (7.84)	179.8	59.9 (3.82)	29.8 (1.80, 1.80)	C^γ 27.4 (1.68, 1.41); C^δ 43.5 (3.09)
F86	118.8 (8.50)	178.3	59.5 (4.50)	38.1 (3.45, 3.01)	C^δ 130.8 (7.20), C^ϵ 131.7 (7.37), C^ζ 130.0 (7.35)
L87	120.1 (8.79)	179.0	58.4 (4.16)	42.6 (2.29, 1.62)	C^γ 26.3 (2.37); C^δ 27.5 (1.10), 23.5 (1.02)
K88	118.8 (8.18)	179.3	60.2 (3.84)	32.3 (1.63, 1.63)	C^γ 25.2 (0.80, 0.18); C^δ 29.5 (1.38, 1.31); C^ϵ 41.8 (2.62, 2.36)
R89	120.3 (7.69)	178.4	58.9 (4.06)	30.3 (2.03, 2.03)	C^γ 26.7 (1.80, 1.67); C^δ 43.6 (3.17)
L90	120.2 (8.51)	177.8	58.0 (4.14)	42.2 (1.84, 1.75)	C^γ 26.5 (1.72); C^δ 26.8 (0.89), 24.9 (0.84)
D91	117.3 (8.35)	175.7	57.6 (4.33)	41.8 (3.33, 3.19)	
R92	114.9 (7.57)	179.9	59.3 (4.10)	29.7 (2.03, 1.99)	C^γ 27.2 (1.81, 1.78); C^δ 43.1 (3.24)
N93	116.8 (8.24)	177.5	56.2 (4.62)	39.5 (2.75, 2.49)	N^δ 112.5 (7.21, 6.85)
L94	121.8 (8.83)	178.4	58.3 (3.88)	42.4 (2.19, 1.63)	C^γ 27.3 (1.79); C^δ 26.4 (0.88), 23.5 (0.69)
W95	119.2 (9.15)	180.2	60.5 (4.29)	29.1 (3.43, 3.39)	$C^{\delta 2}$ 127.5 (7.28); $C^{\epsilon 3}$ 120.2 (7.60); $C^{\zeta 2}$ 114.9 (7.44); $C^{\zeta 3}$ 123.0 (7.27); C^η 124.8 (7.20); $N^{\epsilon 1}$ 129.3 (9.97)
G96	105.7 (8.06)	175.8	46.6 (4.03, 3.85)		
L97	121.2 (7.69)	178.6	56.6 (4.20)	42.7 (1.65, 1.58)	C^γ 26.5 (1.67); C^δ 24.8 (0.58), 24.2 (0.58)
A98	119.6 (7.95)	178.0	54.1 (4.26)	20.1 (1.61)	
G99	101.7 (7.57)	174.0	46.2 (3.82, 3.70)		
L100	118.4 (7.54)	176.1	53.6 (4.41)	44.2 (1.45)	C^γ 26.8 (1.49); C^δ 24.8 (0.85), 23.4 (0.85)
N101	116.9 (8.43)	175.2	53.7 (4.88)	39.6 (2.74, 2.74)	N^δ 108.5 (7.21, 6.95)
S102	111.8 (7.50)	173.1	57.4 (4.67)	63.8 (3.83, 3.83)	
C103	118.7 (8.92)	170.5	54.4 (5.00)	47.3 (3.52, 3.10)	
P104	106.0	176.7	63.2 (4.34)	32.1 (2.26, 1.81)	C^γ 27.4 (2.04, 1.95); C^δ 50.1 (3.70, 3.61)
V105	122.7 (8.39)	175.4	61.4 (4.15)	34.0 (1.96)	C^δ 21.3 (1.01), 21.5 (0.84)
K106	128.1 (8.43)	175.8	55.4 (4.40)	33.0 (1.81, 1.69)	C^γ 24.6 (1.38); C^δ 28.9 (1.67); C^ϵ 41.8 (3.00)
E107	123.3 (8.39)	175.6	57.3 (4.18)	29.7 (1.99, 1.90)	C^γ 36.1 (2.28, 2.28)
A108	125.3 (7.95)	176.7	51.8 (4.49)	19.0 (1.38)	
D109	119.8 (8.03)	175.3	55.0 (4.63)	41.4 (2.83, 2.65)	
Q110	118.7 (8.71)	176.1	54.7 (5.10)	32.4 (2.04, 2.04)	C^γ 33.9 (2.37, 2.37); N^ϵ 113.7 (7.33, 6.60)
S111	115.9 (9.12)	174.2	55.9 (5.05)	66.7 (4.00, 3.72)	
T112	113.6 (8.93)	176.7	62.1 (4.46)	70.4 (4.75)	C^γ 22.2 (1.42)
L113	125.3 (8.90)	178.4	58.2 (4.00)	39.5 (1.80, 0.97)	C^γ 26.2 (1.37); C^δ 22.6 (0.35), 25.5 (0.18)
E114	117.0 (8.52)	177.6	59.8 (3.97)	29.0 (2.10, 1.97)	C^γ 34.6 (2.37, 2.37)
N115	117.8 (7.90)	177.5	56.2 (4.46)	38.5 (2.89, 2.81)	N^δ 112.3 (7.69, 6.92)
F116	123.0 (8.41)	177.1	61.1 (4.43)	40.0 (3.49, 3.00)	C^δ 132.3 (7.23); C^ϵ – (7.36); C^ζ – (7.35)
L117	117.9 (8.91)	179.0	57.6 (3.93)	41.5 (2.10, 1.18)	C^γ 26.5 (2.12); C^δ 26.3 (0.81), 22.4 (0.83)
E118	118.8 (7.96)	179.4	59.2 (4.02)	28.8 (2.17, 2.12)	C^γ 35.0 (2.41, 2.41)
R119	121.0 (7.95)	178.8	58.5 (3.90)	28.7 (1.60, 1.22)	C^γ 26.7 (1.23); C^δ 42.7 (3.06, 2.98)
L120	119.6 (8.10)	177.9	57.3 (3.83)	41.7 (1.78, 1.49)	C^γ 26.7 (1.60); C^δ 25.8 (0.95), 23.3 (0.95)
K121	119.6 (8.49)	177.8	60.5 (3.67)	32.0 (2.12, 1.81)	C^γ 25.2 (1.45, 1.33); C^δ 29.6 (1.75, 1.60); C^ϵ 41.4 (2.88)
T122	116.2 (7.93)	176.4	67.0 (3.84)	68.6 (4.29)	C^γ 21.5 (1.22)
I123	121.4 (7.73)	178.9	64.9 (3.87)	38.4 (1.92)	C^γ 28.9 (1.59, 1.15); $C^{\gamma m}$ 16.7 (1.04), C^δ 14.2 (0.69)
M124	117.9 (8.42)	178.6	56.7 (4.46)	30.4 (2.08, 1.78)	C^γ 32.6 (2.74, 2.35); C^ϵ 17.4 (1.55)
R125	119.9 (8.60)	179.1	59.7 (4.02)	29.8 (1.98)	C^γ 27.8 (1.82, 1.64); C^δ 43.3 (3.22)
E126	119.7 (7.88)	178.8	59.3 (4.15)	29.0 (2.21, 2.15)	C^γ 36.0 (2.47, 2.47)
K127	118.8 (7.92)	178.7	58.8 (4.16)	32.5 (1.99, 1.89)	C^γ 24.6 (1.67, 1.46); C^δ 28.8 (1.67); C^ϵ 41.8 (3.04)
Y128	119.5 (8.50)	177.4	59.2 (4.60)	38.8 (3.14, 3.00)	C^δ 133.2 (7.08); C^ϵ 118.0 (6.79)
S129	115.0 (8.08)	175.6	61.1 (4.21)	63.0 (4.06, 4.06)	
K130	118.9 (7.60)	177.1	56.9 (4.35)	32.2 (1.98, 1.87)	C^γ 24.9 (1.59, 1.49); C^δ 28.8 (1.69); C^ϵ 41.8 (3.01)
C131	115.8 (7.75)	174.2	55.6 (4.77)	41.7 (3.15, 3.11)	
S132	116.0 (7.94)	173.5	58.3 (4.47)	63.9 (3.82, 3.67)	
S133	123.0 (7.76)	178.5	60.1 (4.31)	64.8 (3.87, 3.87)	

[a] In each column, ^{15}N and ^{13}C shifts are listed first, and the corresponding ^{1}H shifts are given in parentheses. ^{1}H and ^{13}C chemical shifts are reported relative to 3-(trimethylsilyl)propionic-d_4 acid and ^{15}N shifts relative to external liquid NH$_3$.

chemical shifts of 54.96 and 59.62 ppm. The resolution in the planes at $\delta^{13}C(F_1)$ = 54.96 ppm is clearly excellent. Further, even though there is some degree of overlap, as in the case of Glu-114, Glu-118, and Glu-126, in the planes at $\delta^{13}C(F_1)$ = 59.62 ppm which corresponds to one of the most crowded $^{13}C^\alpha$ regions of the spectrum, the overall chemical shift dispersion is still reasonable.

To overcome problems associated with chemical shift overlap in the triple-resonance spectra and to substantiate and confirm unambiguously the backbone assignments, it was essential to simultaneously assign the side-chain ^{13}C and ^{1}H resonances using the HCCH-COSY and HCCH-TOCSY spectra. Some typical $^1H(F_1)$–$^1H(F_3)$ slices at two different ^{13}C (F_2) chemical shifts of the HCCH-COSY and HCCH-TOCSY spectra are shown in Figure 5. As is evident from these examples, the HCCH-COSY and HCCH-TOCSY experiments are of very high quality and enabled us to assign >98% of the side-chain ^{13}C and ^{1}H chemical shifts (cf. Table III). Thus, for example, complete spin systems of many of the long side chains (e.g., Leu, Ile, Arg, Lys, and Pro) could easily be identified from the relayed connectivities in the HCCH-TOCSY spectrum, while direct and relayed correlations could be unambiguously

distinguished by comparison with the HCCH-COSY spectrum.

The supplementary connectivities obtained from the three new triple-resonance experiments, namely, the H(CA)NH, HNHB, and HN(CO)HB spectra, played an important role in confirming, as well as establishing, the assignments. In particular, the correlations from the ^{15}N/NH resonances to the $C^{\alpha}H(i,i-1)$, $C^{\beta}H(i)$, and $C^{\beta}H(i-1)$ resonances in these three experiments provide another avenue, in addition to the correlations to the $C^{\alpha}(i,i-1)$ resonances seen in the HNCA and HN(CO)CA spectra, for linking the triple-resonance data with the HCCH-COSY and HCCH-TOCSY data.

Completeness of Scalar Sequential Connectivities. Figure 6 provides a complete summary of the scalar sequential connectivities observed in the 3D triple-resonance experiments. In the vast majority of cases (88%) there are either four (42%) or five (46%) independent sequential scalar connectivities observed between successive residues. Indeed, there are only five, four, and seven cases where one, two, or three out of the five sequential connectivities, respectively, are observed. Thus, these experiments provide numerous cross-checks on the correctness of the assignments. The only scalar correlation that is sparse is the $C^{\beta}H(i)$–$N(i+1)$–$NH(i+1)$ correlation which is observed in only 69 out of a possible 132 times. This is due to the fact that this correlation relies on the three-bond $^{3}J_{COH\beta}$ coupling and can therefore only be generally observed when the $C^{\beta}H$ proton is trans to the backbone carbonyl; that is to say, when the rotamer configuration about the C^{α}-C^{β} bond is either $g^{2}g^{3}$ ($\chi_1 = 60 \pm 30°$) or $g^{2}t^{3}$ ($\chi_1 = 180 \pm 30°$). Further, because the triple-resonance experiments rely entirely on well-defined scalar correlations, potential pitfalls associated with the use of through-space connectivities observed in NOESY spectra, such as the distinction between intraresidue and sequential interresidue and between sequential and nonsequential connectivities, are completely avoided.

Comparison with the Assignments of Redfield et al. (1991). As mentioned in the introduction, Redfield et al. (1991) have recently published a preliminary set of ^{15}N and ^{1}H backbone assignments making use of 3D ^{15}N-edited NOESY and HOHAHA spectra in combination with conventional 2D ^{1}H–^{1}H correlation spectroscopy. Although their data were collected under slightly different conditions from those employed in this paper (pH 5.3 as opposed to pH 5.7), there seems to be excellent agreement between the two sets of data. In this regard, it is interesting to note that, even for the two regions where single amino acid substitutions are present between the two sequences, namely, Asp-42 → Asn and Asp-108 → Asn (using the current numbering scheme), the backbone ^{15}N and ^{1}H chemical shifts for these two residues, as well as the three preceding and following ones, are very similar indeed, differing by less than 0.1 ppm for protons and 1 ppm for ^{15}N.

Concluding Remarks

In this paper we have described the use of a series of 3D double- and triple-resonance NMR experiments to determine near complete ^{1}H, ^{15}N, ^{13}C, and ^{13}CO assignments of IL-4, a protein exhibiting an unusual degree of chemical shift degeneracy and overlap, owing to its very high degree of helical character. This information is absolutely essential for the determination of both the secondary and tertiary structures of this protein. The latter will be primarily based on data derived from 4D ^{15}N/^{13}C- and ^{13}C/^{13}C-edited NOESY spectroscopy (Kay et al., 1990b; Clore et al., 1991b), which, in the case of proteins larger than about 15 kDa, have proved to be essential for obtaining the very large number of approximate interproton distance restraints required for a high-resolution structure determination (Clore et al., 1991c; Clore & Gronenborn, 1991c). The data presented in this paper should permit the semiautomated identification of NOEs in the 4D spectra in a relatively straightforward manner.

The large number of scalar sequential correlation pathways provided by the 3D triple-resonance experiments (cf. Figure 6), coupled with the extensive side-chain assignments provided by the HCCH-COSY and HCCH-TOCSY experiments, remove all ambiguities and permit the assignment of resonances with complete confidence. Further, the data are of sufficient resolution to permit assignment by semiautomated methods, which significantly simplifies and speeds up the process. Moreover, it also alleviates problems associated with limited chemical shift dispersion encountered in α-helical proteins, as well as the need to rely heavily on tentative ^{1}H side-chain spin assignments derived from a 3D ^{15}N-edited NOESY spectrum (Redfield et al., 1991), a procedure fraught with difficulties. The fact that the partial set of assignments reported by Redfield et al. (1991) are in agreement is a testament to the great care and obvious attention for detail taken by the Oxford group.

References

Archer, S. J., Ikura, M., Sporn, M. B., Torchia, D. A., & Bax, A. (1991) *J. Magn. Reson. 95*, 636–641.

Bax, A. (1989) *Methods Enzymol. 176*, 151–158.

Bax, A. (1992) *Curr. Opin. Struct. Biol. 1*, 1030–1035.

Bax, A., Clore, G. M., Driscoll, P. C., Gronenborn, A. M., Ikura, M., & Kay, L. E. (1990a) *J. Magn. Reson. 87*, 620–628.

Bax, A., Clore, G. M., & Gronenborn, A. M. (1990b) *J. Magn. Reson. 88*, 425–431.

Bax, A., Ikura, M., Kay, L. E., Torchia, D. A., & Tschudin, R. (1990c) *J. Magn. Reson. 86*, 304–318.

Clore, G. M., & Gronenborn, A. M. (1987) *Protein Eng. 1*, 275–288.

Clore, G. M., & Gronenborn, A. M. (1989) *Crit. Rev. Biochem. Mol. Biol. 24*, 479–564.

Clore, G. M., & Gronenborn, A. M. (1991a) *Annu. Rev. Biophys. Biophys. Chem. 20*, 29–63.

Clore, G. M., & Gronenborn, A. M. (1991b) *Progr. Nucl. Magn. Reson. Spectrosc. 23*, 43–92.

Clore, G. M., & Gronenborn, A. M. (1991c) *Science 252*, 1390–1399.

Clore, G. M., Bax, M., Driscoll, P. C., Wingfield, P. T., & Gronenborn, A. M. (1990) *Biochemistry 29*, 8172–8184.

Clore, G. M., Bax, A., & Gronenborn, A. M. (1991a) *J. Biomol. Nucl. Magn. Reson. 1*, 13–22.

Clore, G. M., Kay, L. E., Bax, A., & Gronenborn, A. M. (1991b) *Biochemistry 30*, 12–18.

Clore, G. M., Wingfield, P. T., & Gronenborn, A. M. (1991c) *Biochemistry 30*, 2315–2323.

Clubb, R. T., Thanabal, V., Osborne, C., & Wagner, G. (1991) *Biochemistry 30*, 7718–7730.

Curtis, B. M., Presnell, S. R., Srinivasan, S., Sassenfeld, H., Klinke, R., Jeffery, E., Cosman, D., March, C. J., & Cohen, F. E. (1991) *Proteins: Struct. Funct., Genet. 11*, 111–119.

Delaglio, F., Torchia, D. A., & Bax, A. (1991) *J. Biomol. Nucl. Magn. Reson. 1*, 439–446.

Golumbek, P. T., Lazenby, A. J., Levitzky, H. I., Jaffee, L. M., Karasuyama, H., Baker, M., & Pardoll, D. M. (1991) *Science 254*, 713-716.

Driscoll, P. C., Clore, G. M., Marion, D., Wingfield, P. T., & Gronenborn, A. M. (1990a) *Biochemistry 29*, 3542-3556.

Driscoll, P. C., Gronenborn, A. M., Wingfield, P. T., & Clore, G. M. (1990b) *Biochemistry 29*, 4668-4682.

Dyson, H. J., Gippert, G. P., Case, D. A., Holmgren, A., & Wright, P. E. (1990) *Biochemistry 29*, 4129-4136.

Fairbrother, W. J., Cavanagh, J., Dyson, H. J., Palmer, A. G., Sutrina, S. L., Reizer, J., Saier, M. H., & Wright, P. E. (1991) *Biochemistry 30*, 6896-6907.

Fieschko, J. C., Egan, K. M., Ritch, T., Koski, R. A., Jones, M., & Bitter, G. (1987) *Biotechnol. Bioeng. 29*, 1113-1121.

Fesik, S., & Zuiderweg, E. R. P. (1988) *J. Magn. Reson. 78*, 588-593.

Fesik, S., & Zuiderweg, E. R. P. (1990) *Q. Rev. Biophys. 23*, 97-131.

Forman-Kay, J. D., Clore, G. M., Wingfield, P. T., & Gronenborn, A. M. (1991) *Biochemistry 30*, 2685-2698.

Garrett, D. S., Powers, R., Gronenborn, A. M., & Clore, G. M. (1991) *J. Magn. Reson. 95*, 214-220.

Grzesiek, S., Ikura, M., Clore, G. M., Gronenborn, A. M., & Bax, A. (1992) *J. Magn. Reson. 96*, 215-222.

Ikura, M., & Bax, A. (1991) *J. Biomol. Nucl. Magn. Reson. 1*, 99-104.

Ikura, M., Kay, L. E., & Bax, A. (1990a) *Biochemistry 29*, 4659-4667.

Ikura, M., Kay, L. E., Tschudin, R., & Bax, A. (1990b) *J. Magn. Reson. 86*, 204-209.

Ikura, M., Kay, L. E., Krinks, M., & Bax, A. (1991) *Biochemistry 30*, 5498-5504.

Kay, L. E., Marion, D., & Bax, A. (1989) *J. Magn. Reson. 84*, 72-84.

Kay, L. E., Ikura, M., Tschudin, R., & Bax, A. (1990a) *J. Magn. Reson. 89*, 496-514.

Kay, L. E., Clore, G. M., Bax, A., & Gronenborn, A. M. (1990b) *Science 249*, 411-414.

Kay, L. E., Ikura, M., & Bax, A. (1991) *J. Magn. Reson. 91*, 84-92.

Marion, D., & Bax, A. (1988b) *J. Magn. Reson. 80*, 528-533.

Marion, D., Kay, L. E., Sparks, S. W., Torchia, D. A., & Bax, A. (1989a) *J. Am. Chem. Soc. 11*, 1515-1517.

Marion, D., Driscoll, P. C., Kay, L. E., Wingfield, P. T., Bax,

A., Gronenborn, A. M., & Clore, G. M. (1989b) *Biochemistry 28*, 6150-6156.

Marion, D., Ikura, M., Tschudin, R., & Bax, A. (1989c) *J. Magn. Reson. 85*, 393-399.

Messerle, B. A., Wider, G., Otting, G., Weber, C., & Wüthrich, K. (1989) *J. Magn. Reson. 85*, 608-613.

Norwood, T. J., Boyd, J., Heritage, J. E., Soffe, N., & Campbell, I. D. (1990) *J. Magn. Reson. 87*, 488-501.

Oschkinat, H., Griesinger, C., Kraulis, P. J., Sørensen, O. W., Ernst, R. R., Gronenborn, A. M., & Clore, G. M. (1988) *Nature (London) 332*, 374-377.

Park, L. S., Friend, D., Sassenfeld, H. M., & Urdal, D. L. (1987) *J. Exp. Med. 166*, 476-488.

Paul, W. E., & Ohara, J. (1987) *Annu. Rev. Immunol. 5*, 429-460.

Pelton, J. G., Torchia, D. A., Meadow, N. D., Wong, C.-W., & Roseman, S. (1991) *Biochemistry 30*, 10043-10057.

Powers, R., Gronenborn, A. M., Clore, G. M., & Bax, A. (1991) *J. Magn. Reson. 94*, 209-213.

Powers, R., Clore, G. M., Bax, A., Garrett, D. S., Stahl, S. J., Wingfield, P. T., & Gronenborn, A. M. (1991b) *J. Mol. Biol. 221*, 1081-1090.

Price, V., Mochizuki, D., March, C. J., Cosman, D., Deeley, M. C., Klinke, R., Clevenger, W., Gillis, S., Baker, P., & Urdal, D. L. (1987) *Gene 55*, 287-293.

Redfield, C., Smith, L. J., Boyd, J., Lawrence, G. M. P., Edwards, R. G., Smith, R. A. G., & Dobson, C. M. (1991) *Biochemistry 30*, 11029-11033.

Tepper, R. I., Pattengale, P. K., & Leder, P. (1989) *Cell 57*, 503-510.

Vuister, G. W., Boelens, R., & Kaptein, R. (1988) *J. Magn. Reson. 80*, 176-185.

Walder, R. Y., & Walder, J. A. (1986) *Cell 42*, 133-139.

Windsor, W. T., Syto, R., Le, H. V., & Trotta, P. P. (1991) *Biochemistry 30*, 1259-1264.

Wüthrich, K. (1986) *NMR of Proteins and Nucleic Acids*, John Wiley, New York.

Wüthrich, K. (1989) *Acc. Chem. Res. 22*, 36-44.

Yokota, T., Arai, N., deVries, J., Spits, H., Banchereau, J., Zlotnik, A., Rennick, D., Howard, M., Takebe, Y., Miyatake, S., Lee, F., & Arai, K. (1988) *Immunol. Rev. 103*, 137-187.

Zhu, G., & Bax, A. (1990) *J. Magn. Reson. 90*, 405-410.